nature machine intelligence

Article

https://doi.org/10.1038/s42256-023-00728-z

A soft-packaged and portable rehabilitation glove capable of closed-loop fine motor skills

Received: 4 January 2023

Accepted: 5 September 2023

Published online: 5 October 2023

Check for updates

Mengli Sui[1,5], Yiming Ouyang[1,5], Hu Jin[1,5] ✉, Zhenyi Chai[1], Changyang Wei[1], Jiyu Li[2,3], Min Xu[1], Weihua Li[4], Liu Wang[2,3] ✉ & Shiwu Zhang[1] ✉

Regaining fine motor skills (FMSs; that is, the ability to make precise and coordinated movements of fingers) is the ultimate goal of hand rehabilitation. Although robotic-assisted technologies have been widely explored to help patients with simple hand activities, existing rehabilitation gloves still lack sensory feedback for closed-loop control or involve bulky external hardware, incapable of providing precise FMSs rehabilitation portably. Here we develop a soft rehabilitation glove that can accomplish diverse FMSs by integrating 15 bending sensors and 10 shape-memory-alloy (SMA) actuators. Three joint angles of each finger can be precisely sensed and thus are fed to the control system to actuate SMAs in a closed-loop manner. A touchable human–machine interface is also integrated to provide facile interaction for multi-modal rehabilitation exercises. Weighing only 0.49 kg, our soft glove has high portability, allowing for repetitive hand rehabilitation as needed. We validate that our glove can assist an individual with hand impairments after a stroke to realize a set of single and complex FMS rehabilitation exercises and to complete some activities of daily living.

Each year, there are over 7 million new patients with hand disabilities worldwide after a stroke[1]. Due to impaired neural pathways[2], afflicted patients lose the ability to make precise, voluntary and coordinated movements of fingers—referred to as fine motor skills (FMSs). Neuroplasticity theory suggests that repetitive and consistent practices of hand motion can rewire the neural pathways that modulate hand functions[3–6]. Therefore, patients usually take intensive rehabilitation training with professional therapists in the hospital[7,8]. However, traditional rehabilitation therapy often involves high medical costs for patients and heavy workloads for therapists[9].

To address this issue, recent decades have seen substantial interest in developing robotic-assisted technologies that help patients perform rehabilitation training[10–17]. Consisting of rigid structures (for example, metallic rods), many existing rehabilitation devices (for example, ExoK'ab exoskeleton[18] and Haptic Knob end-effector[19]) are still bulky and heavy, limiting rehabilitation training to only hospitals and possessing potential risks of injuring the finger[20]. As a result, soft hand rehabilitation gloves are rapidly emerging owing to their lower weight and safer human–machine interaction[21–27]. For example, hydraulic/pneumatic[28–34] and motor-cable[35,36] soft gloves that use soft tubes and cables to bend fingers have been widely studied and commercialized. Despite the reduced weight of the glove itself, external hardware (for example, pump + tubes, motor + cables) is still required for actuation[32–34], making the entire system heavier[37–42] (Supplementary Table 1).

Recently, shape-memory-alloy (SMA, for example, TiNi alloy) actuators represent a prominent candidate for creating a portable glove system. The driving force originates from the heating-induced transformation from the martensite phase to the austenite phase. Due to their high power-to-weight ratio, large deforming capability, relatively low driving voltage and noiseless actuation, SMAs have been

[1]CAS Key Laboratory of Mechanical Behavior and Design of Materials, Department of Precision Machinery and Precision Instrumentation, University of Science and Technology of China, Hefei, China. [2]CAS Key Laboratory of Mechanical Behavior and Design of Materials, Department of Modern Mechanics, University of Science and Technology of China, Hefei, China. [3]State Key Laboratory of Nonlinear Mechanics, Institute of Mechanics, Chinese Academy of Science, Beijing, China. [4]School of Mechanical, Materials, Mechatronic and Biomedical Engineering, University of Wollongong, Wollongong, New South Wales, Australia. [5]These authors contributed equally: Mengli Sui, Yiming Ouyang, Hu Jin. ✉e-mail: jhrdsp@ustc.edu.cn; wangliu05@ustc.edu.cn; swzhang@ustc.edu.cn

extensively adopted as actuators in robotics fields[43–51]. In particular, several groups have reported potential applications of SMAs in hand rehabilitation[52,53]. However, existing rehabilitation gloves are still facing the grand challenge of accomplishing FMSs with precision[14,54–56]. The main reasons are twofold[54]. First, most gloves are not equipped with sensors that are directly mounted to impaired fingers to precisely capture their deformation. For example, some commercial products (for example, Vrehab-M2 and Mirror Hand) use bending sensors only on the healthy hand to detect the mirror motion for the training. Second, they do not have closed-loop control of the finger during the bending process, especially when coordinating multiple fingers to complete complex FMSs (Supplementary Table 1).

Here we present a soft-packaged and portable rehabilitation glove that is capable of diverse FMSs with real-time sensory feedback and a close-loop control system (Fig. 1a and Supplementary Video 1). Consisting of two Hall sensors, one magnet and a thin wire connecting the joint, three bending sensors are customized and deployed on each finger to precisely detect three joint angles (Fig. 1b). The sensory feedback is then processed by the control circuit board to heat SMA actuators in a closed-loop manner. The soft fingerstall is biomimetically engineered with wrinkle-like serpentine structures to enable large stretchability over joints and a dual-SMA actuating system is designed and optimized with minimal backlash. A touchable control panel, together with an integrated battery (0.15 kg), is directly mounted on the forearm to provide facile human–machine interaction for multi-modal rehabilitation exercises (Fig. 1c). Our soft-packaged glove weighs only 0.49 kg with high compactness, portability and low noise, giving rise to more opportunities for repetitive rehabilitation in various environments such as in an office and a park (Fig. 1d,e). We validate that our glove can assist an individual after a stroke with hand impairments to complete both single-mode and switch-mode FMSs. Our soft glove also paves the way for assisting the individual with daily tasks such as closing the door, watering flowers and brushing teeth (Fig. 1e).

Results

General design and working principle

Our soft glove consists of three major modules: a touchable HMI panel, a control and actuation system, and biomimetic fingerstalls with bending sensors (Fig. 2a,b). The human–machine interface (HMI) panel is the portal for inputting the command of desired FMS rehabilitation while displaying the actual status of the fingers in real time (Fig. 2c). A list of FMS rehabilitation exercises is pre-programmed and can be readily accessed by clicking corresponding buttons on the HMI (Supplementary Fig. 1 and Supplementary Video 2). Once the command of desired FMS rehabilitation is received by the control system, it generates ten-channel pulse-width-modulation (PWM) waves to actuate ten SMA springs that control five fingers (Supplementary Fig. 2). By heating the SMA actuator with an integrated battery (12 V) to its austenite phase finish temperature (A_f = 90 °C), the SMA spring contracts quickly, yielding an averaged contacting force of 7 N (equivalent stress 34 MPa; Supplementary Fig. 3). In a grasping test, the maximum force exerted by the fingertip is 14.3 N (Supplementary Video 3). The SMA shows excellent mechanical stability in 10,000 cycles of heating and cooling at stress of 34 MPa (variation <2%; Supplementary Fig. 4). The energy density and energy efficiency of the SMA is measured as 2,558 J kg^{-1} and 3.23% (1.11% for glove due to friction and so on), respectively (Supplementary Fig. 5), which agree with typical values reported in the literature[57,58]. The contracting force is then transmitted to a finger via a pair of cables: a bending cable and a flattening cable as highlighted by red lines. To bend the finger, the bending cable passes through two straps (one for the thumb) and is attached to the fingertip on the bottom side of the fingerstall. Similarly, the flattening cable is attached to the fingertip through a set of small holes on the top side of the fingerstall. Three customized bending sensors are mounted on the phalanges (that is, finger bones) to capture three joint angles (denoted as φ_m, φ_p and φ_d) at a sampling rate of 200 Hz. The bending angle of the finger (defined as $\varphi = \varphi_m + \varphi_p + \varphi_d$) will be controlled in a closed-loop manner to eventually achieve the desired value. A cooling system consists of a fan and five pairs of motor switches (unit weight 2 g) built in to selectively cool a designated SMA when the airway is open, while other SMAs remain unaffected when the airway is closed (Supplementary Fig. 6). When the fan is working, the measured noise is 55 dB, which is lower than pneumatic pumps and motors (Supplementary Table 3 and Supplementary Video 4). Note that the maximum temperature on the cover of the working glove is 37.7 °C, which is safe for a human to wear on the arm (Supplementary Fig. 7). A hole is reserved at the fingertip to provide the touch sensitivity of fingertip (Fig. 2b). The entire glove only weighs 0.49 kg (battery ~0.15 kg) with a lower cost than the existing commercial products (Supplementary Table 1).

Biomimetic design of fingerstall with joint angle sensing capability

Human fingers, excluding the thumb, consist of three phalanges, namely, the distal phalange, middle phalange and proximal phalange, from the tip to the root of the finger. The bending behaviour of the finger is enabled by three joints, known as metacarpophalangeal (MCP), proximal interphalangeal (PIP) and distal interphalangeal (DIP) joints, respectively (Fig. 3a). Upon bending, the wrinkled skin on top of each joint is markedly stretched, allowing for three joint angles (φ_m, φ_p and φ_d in Fig. 3a), respectively. A key component of the soft glove is the fingerstall that wraps around the finger to transmit force and enable movement. To accommodate the large bending behaviour while providing stable sensory feedback of joint angles, two principles are adopted in designing the fingerstall. First, the joint portions should have a high stretchability comparable to wrinkled skin. Second, bending sensors should be mounted at locations with minimal deformation to eliminate movement artefacts. Here we adopt an index finger as a representative model to elucidate design principles. Notably, these design principles are also applicable to other fingers except that the thumb has different bone structures (Supplementary Fig. 8).

The strain distribution of the skin on top of the index finger at the deformed configuration is first investigated (Fig. 3a). The flat finger is the reference configuration where a far enough point O is selected to be the origin. A point of interest Q is characterized by the length L and S with respect to origin O in reference and deformed configurations, respectively. After deformation, the strain at point Q is

$$\varepsilon = \frac{\mathrm{dS} - \mathrm{dL}}{\mathrm{dL}} \tag{1}$$

where dL and dS represent the infinitesimal increment in the reference and deformed configurations, respectively. By setting dL = 5 mm in experimental measurements (see the red marker on the finger in Fig. 3a), the strain ε can be approximately discretized and calculated according to equation (1). Figure 3b plots the strain distribution as a function of reference position L when the finger bends to the utmost (that is, maximum φ_m = 70°, φ_p = 100° and φ_d = 60°). The inset in Fig. 3b shows the length of MCP, PIP and DIP joints before and after bending.

Following the first design principle, we engineer the joint portions of the fingerstall to be serpentine structures that mimic the biological wrinkle of the skin. As MCP and PIP have a similar reference length (~15 mm) that is larger than DIP (~10 mm), a serpentine with three periods is adopted for MCP and PIP joints, while the DIP joint is designed with two periods (Fig. 3c and Supplementary Fig. 9). The large stretchability of three joints is validated by finite element analysis (FEA) in Fig. 3d where the local strain is shown. Although the entire serpentine is largely stretched, local strains are quite small (blue regions) except for the boundary of serpentine crests, manifesting the large stretchability of the fingerstall to accommodate the finger's bending. Complying with the second design principle, three bending sensors are placed

https://doi.org/10.1038/s42256-023-00728-z

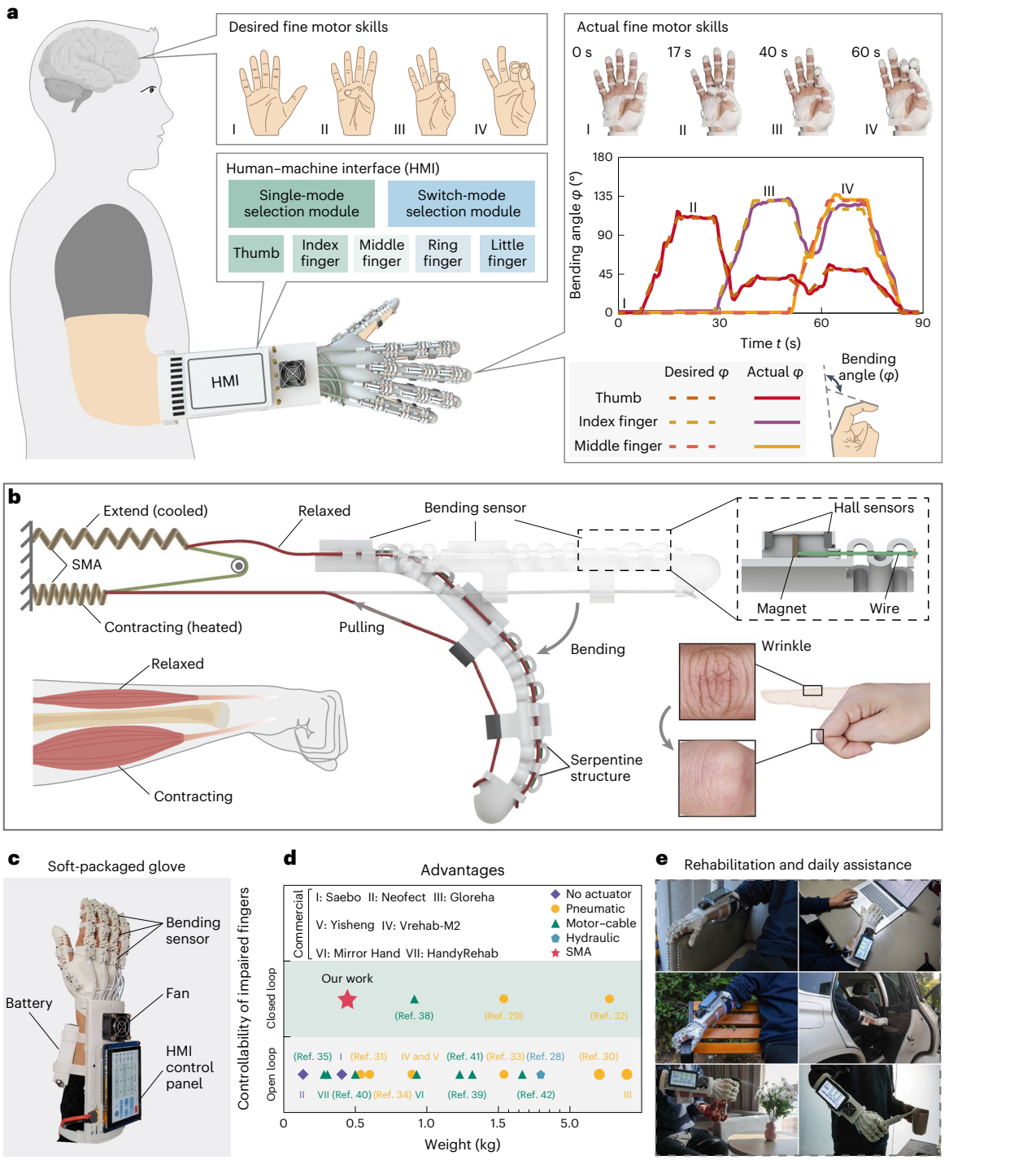

Fig. 1 | A soft-packaged and portable rehabilitation glove capable of closed-loop FMSs. a, An overview showing that the soft glove assists an individual with hand impairments to accomplish a set of desired FMSs with precise bending angles of involved fingers. The highly packaged glove can be mounted on the forearm of the individual with a touchable HMI for facile control of multi-modal FMS rehabilitation. The bending angle of the finger is denoted as φ. **b**, Schematic illustration of the biomimetic design of the dual-SMA actuating system and fingerstall structures with sensing capability. One SMA is heated to contract while the other remains in a cooled state. The wrinkle-like serpentine structure enables a large stretchability of the fingerstall over joints. Three joint angles are accurately sensed by three customized bending sensors. **c**, Picture of the soft-packaged and portable rehabilitation glove mounted on a human forearm. **d**, Comparison of the controllability and weight between various rehabilitation gloves. Our soft glove has closed-loop control of impaired fingers' motion and lower weight (0.49 kg). **e**, Exemplary images of FMS rehabilitation in different environments (home, office, park) and daily assistance tasks (closing the door, watering flowers, brushing teeth) for an individual after a stroke with hand impairments.

at the phalangeal areas that have small strains (Fig. 3c). Each bending sensor consists of two Hall sensors, one magnet and an encapsulating guideway that allows the magnet to translate freely between two Hall sensors (Supplementary Fig. 10). To detect the joint angle, a thin wire is used to connect the magnet with the rightmost serpentine via a tiny hole. When the joint bends, the serpentine structure stretches, and the thin wire pulls the magnet, changing the output voltage of Hall sensors. Note that the thin wire is made of TiNi alloy (diameter 0.38 mm) that

https://doi.org/10.1038/s42256-023-00728-z

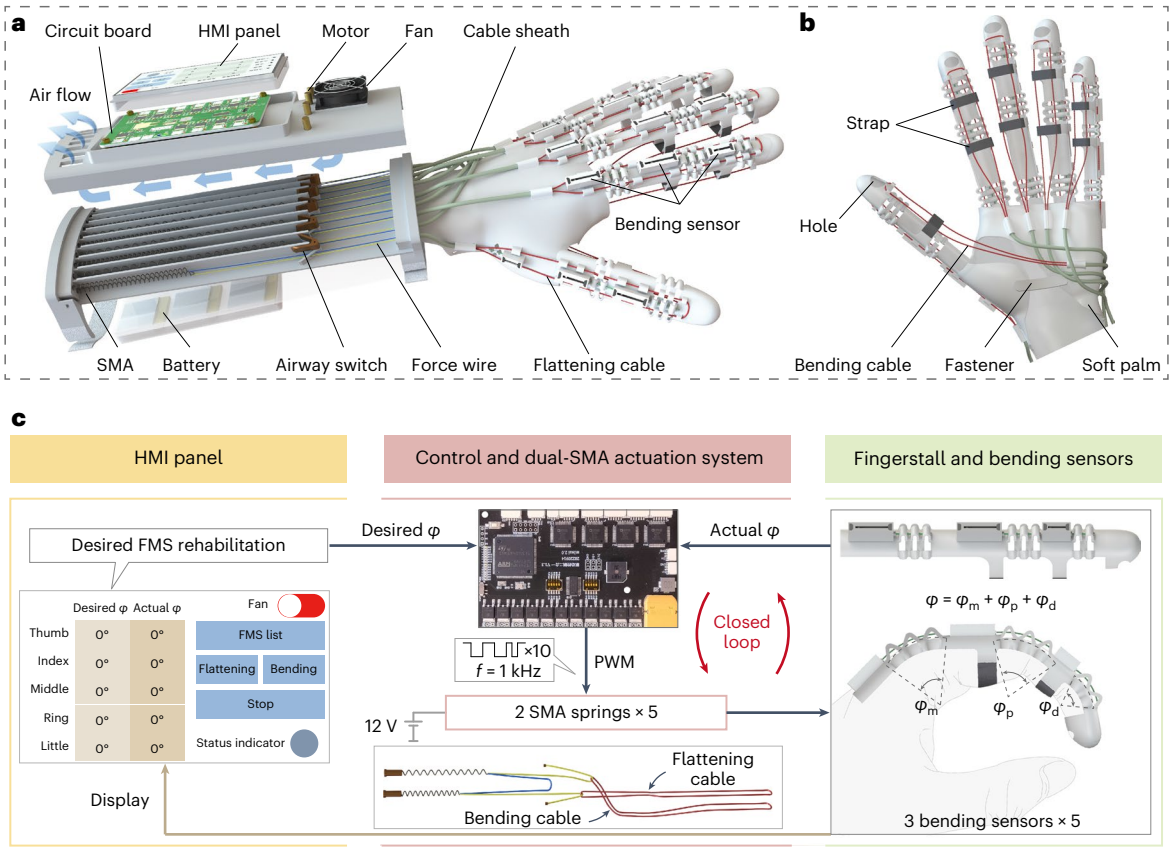

Fig. 2 | General design and working principle of the soft glove. a, An exploded view of the soft glove. By selectively heating (via the battery) the SMA spring actuators, the bending cable and flattening cable pulls the finger to bend and flatten, respectively. A circuit board and HMI panel are integrated for facile control and interaction. Five pairs of motor switches are used to selectively cool designated SMAs. **b**, The back view of the hand portion of the soft glove. The bending cables pass through the small holes of the strap(s) and are attached to the fingertip. A hole is reserved at the fingertip for touch sensitivity. **c**, The working principle of the soft glove in which the command of desired FMS rehabilitation is given to the HMI, processed by the control circuit and executed by the SMA spring actuators to deform the target fingers. The actual bending angle of the finger (denoted as φ) is measured by three bending sensors and is then fed to the circuit board for closed-loop control, while they are displayed on the HMI panel in real time.

can sustain a certain compressive force and the surrounding serpentine structures also prevent buckling instability when compressed (Supplementary Fig. 10c). Therefore, it can readily push the magnet backwards when the joint flattens (Supplementary Video 5), allowing for the detection of the joint angle in reverse motions.

To quantify the relationship between the output voltage and the three joint angles, we build an image-based calibration system that measures three joint angles by processing the image of the deformed finger. We first test this calibration system on a finger phantom (Supplementary Fig. 11a). Notably, the bending sensors have good repeatability after 50 cycles of tests. For the application on a human finger, 50 cycles of tests are adopted to calculate the averaged output voltage in calibration. Results for the index finger are presented in Fig. 3e (normalized by the maximum output voltage) and Supplementary Fig. 11d (absolute output voltage). Therefore, three joint angles can be precisely sensed during the bending process of the finger.

Dual-SMA actuators with minimized backlash

As depicted in Supplementary Fig. 12, a healthy finger is controlled by coordinating a pair of muscles: flexor and extensor. When only the flexor contracts, the finger bends; when only the extensor contracts, the finger flattens. If both muscles exert forces, the finger undergoes abnormal movements. Inspired by this muscle control mechanism, a similar dual-SMA actuating system is designed in which when one SMA is heated to contract, the other remains cooled. To double the actuating force, two force wires (denoted as blue lines in Fig. 4a) are used to connect the SMA and the bending/flattening cable. By connecting two SMA actuators with a connecting wire (illustrated by the green line), the counterforce of the extended cooled SMA is further cancelled, leading the finger to be solely controlled by the heated SMA. For example, when SMA 2 is heated, the bending cable pulls the finger while force wire 1 remains loose (relaxed), and vice versa. If there is no connecting wire, the cooled SMA still exerts a counterforce when extended (maximum value ~2.5 N; see mechanical characterization in Supplementary Fig. 3), causing a jammed finger (Supplementary Fig. 12).

The loose force wire, on the one hand, cancels the transmission of counterforce from the cooled SMA to the finger, allowing the finger to be controlled solely by one cable at one time. On the other hand, it interrupts the transmission of contracting force when the cooled SMA is heated thereafter, delaying the execution of reverse motion. This negative effect is referred to as backlash. Note that force wire 2 is intentionally designed as straight yet tensionless when the finger is flat so that backlash does not occur on force wire 2 when the finger bends from the flat state. Therefore, the backlash only accumulates in force wire 1 during bending, which can be quantified as

$$\Delta b = \Delta s - 2\Delta w \tag{2}$$

where Δs and Δw denote the displacement of SMA 1 and flattening cable, respectively (Fig. 4a). For an ideal design without backlash,

https://doi.org/10.1038/s42256-023-00728-z

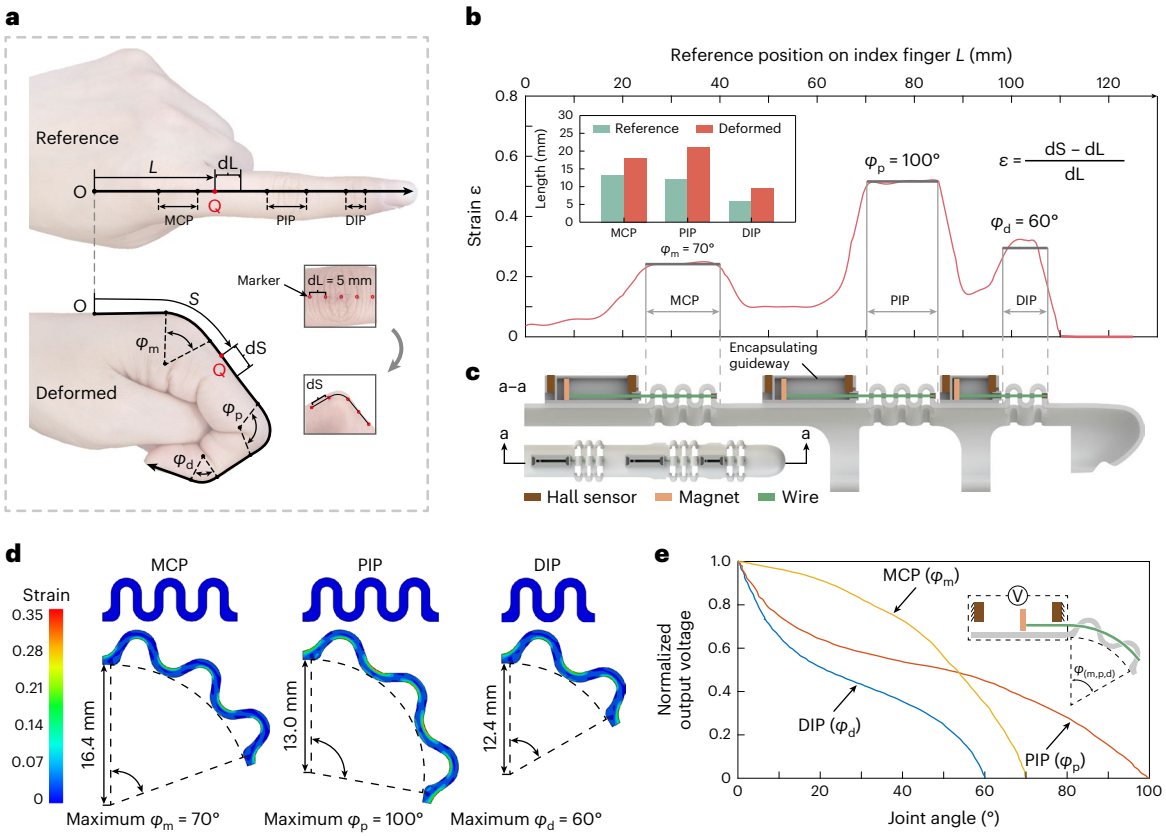

Fig. 3 | Biomimetic design of fingerstall with joint angle sensing capability. **a**, The reference and deformed configuration of the index finger. The skin over joints is highly stretched, which allows for the large joint angles that are denoted as φ_m, φ_p and φ_d for the MCP, PIP and DIP joints, respectively. **b**, The strain distribution of the skin on the index finger when it bends to the utmost configuration where maximum $\varphi_m = 70°$, $\varphi_p = 100°$ and $\varphi_d = 60°$. The inset shows the length of three joints in reference and deformed configurations. **c**, Cross-section view and zoomed-out top view (bottom left) of the fingerstall. The joint portions of the fingerstall are engineered with wrinkle-like serpentine structures with high stretchability. Three bending sensors, consisting of two Hall sensors and one magnet encapsulated in the guideway, are placed at the phalangeal areas that have small strains. The a-a denotes the middle-plane cut view. **d**, FEA results of local strain distribution in three serpentine structures at the maximum joint angle. **e**, The normalized output voltage of bending sensors as a function of the corresponding joint angle.

that is, $\Delta s = 2\Delta w$, force wire 1 remains straight yet tensionless during the bending process (Fig. 4b). Thereafter, when the bent finger begins to flatten, the contracting force by heated SMA 1 can immediately transmit to the flattening cable. With a backlash, SMA 1 needs to contract a bit until the loose force wire 1 becomes straight. Figure 4b depicts five representative states to illustrate backlash in a cycle of bending and flattening. Initially, the finger is flat and two SMAs are cooled. Two force wires are straight without tension (state I). By heating SMA 2, SMA 2 contracts and SMA 1 extends. Force wire 2 is tight and force wire 1 becomes loose (state II). The backlash reaches the maximum value Δb^m when the finger has the largest bending angle $\varphi = 230°$ (state III). Thereafter, by cooling SMA 2 and heating SMA 1, SMA 1 contracts and SMA 2 extends and both force wires become loose (backlash state IV). By further heating SMA 1, the force wire 1 wire becomes straight (state V), pulling the finger back to the flat state (state I).

The backlash, though undesired, can be minimized by optimizing the location of two fingerstall straps. The distance between the strap and adjacent finger joint is denoted as L_m and L_p, respectively (Fig. 4c). The kinematic modelling of the fingerstall is provided in Supplementary Text and Supplementary Fig. 13. By analysing the maximum bending configuration ($\varphi = 230°$), we present normalized backlash $\Delta b^m/\Delta s^m$ as a function of L_m and L_p in Fig. 4c. It is found that reducing L_m and L_p minimizes the backlash. However, for successful hand rehabilitation, the bending torque applied on the joint should be larger than a threshold, that is, $\tau_m > 20$ N cm and $\tau_m > 15$ N cm according to ref. 59. Therefore, $L_m = 4.7$ mm and $L_p = 5.3$ mm is adopted and the minimum $\Delta b^m/\Delta s^m = 9.8\%$ is achieved. Considering that the maximum extension of SMA 1 is $\Delta s^m = 80$ mm, the minimized backlash $\Delta b^m = 7.8$ mm is small enough. It is worth noting that the backlash only delays the execution of reverse motion while the accuracy of the bending finger is guaranteed by the closed-loop control system.

Closed-loop control of bending angle

Figure 4d shows the algorithm of the closed-loop control. Enabled by three bending sensors, three joint angles can be precisely detected at a sampling rate of 200 Hz. Hence, the difference between the desired and actual bending angle (denoted as $\Delta\varphi$) can be calculated in real time. If $\Delta\varphi$ is larger than the tolerance of 2°, a proportional-integral controller with feed-forward compensation is used to automatically adjust the duty ratio of SMA actuators. A detailed control algorithm is provided in Methods and Supplementary Text. Before application on human hands, we first test the dual-SMA actuating system on a finger phantom using the image-based calibration system (Supplementary Fig. 11). Take the maximum bending angle $\varphi = 230°$ as a representative example. Figure 4e shows the bending angle φ and duty ratio as a function of time t. A desired step response (dashed line) is put into the control system at $t = 5$ s and terminates at $t = 15$ s. First, SMA 2 is actuated with a 100% duty ratio, that is, heated at 12 V voltage (state I), and the actuation response time $t_a = 0.7$ s is observed before the finger's

https://doi.org/10.1038/s42256-023-00728-z

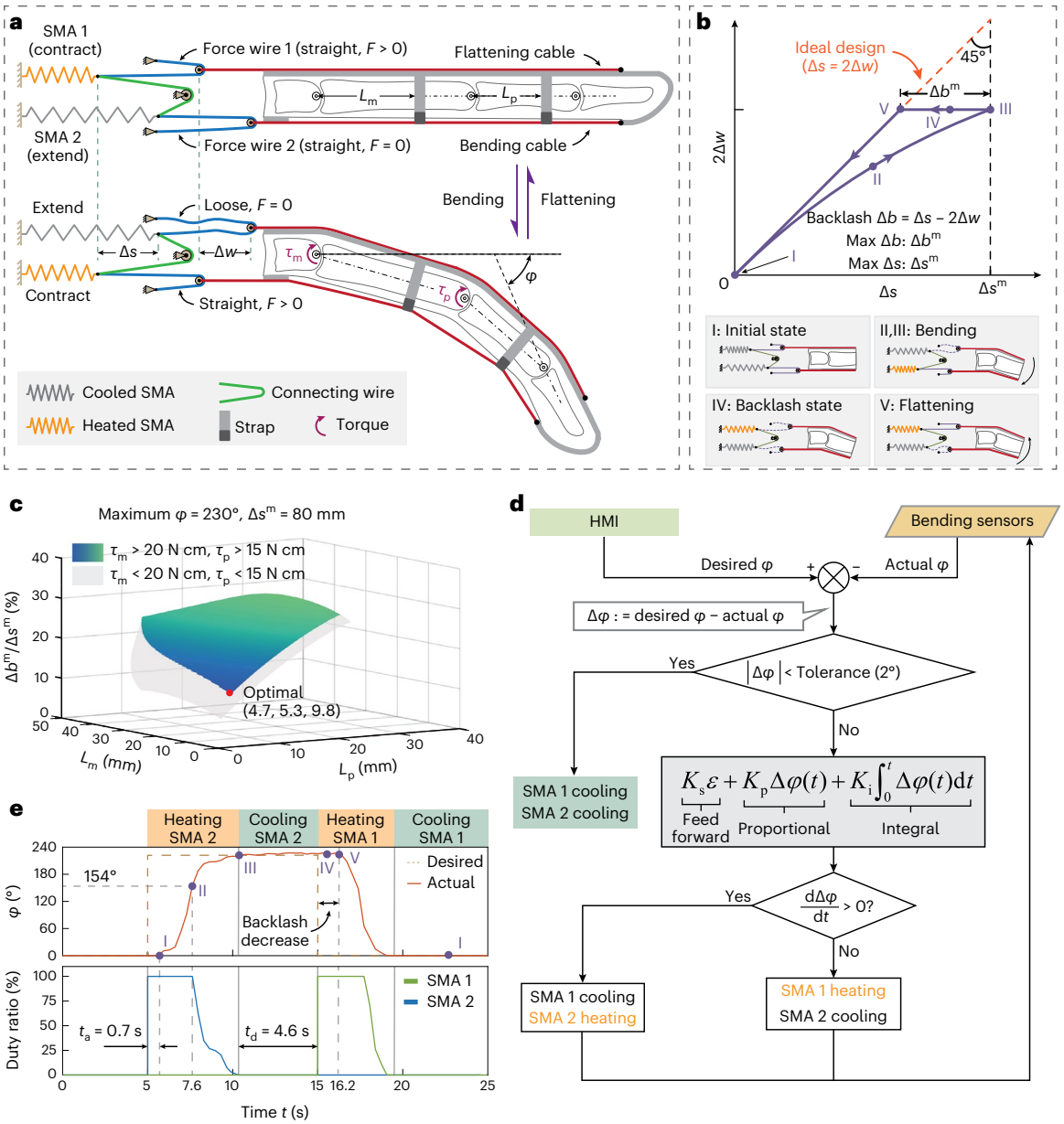

Fig. 4 | Design of dual-SMA actuators with closed-loop controllability. **a**, Schematic model of the dual-SMA actuating system in which one SMA is heated to contract while the other SMA remains cooled. Two SMAs are connected via a connecting wire that allows the finger to be solely controlled by the cable on one side (that is, the force transmission on the other side is cancelled by the loose force wire). The tension in the force wire is denoted as F. **b**, Schematic illustration of backlash during a cycle of bending and flattening. The force wire 1 becomes loose in the bending process, which yields a delay of execution in the flattening process. **c**, Normalized backlash as a function of strap locations (quantified by the distance to the MCP joint L_m and PIP joint L_p in **a**. The optimal locations are determined by minimizing backlash while satisfying torque applied to MCP and PIP joints larger than the threshold. **d**, Flow chart of the closed-loop control of dual-SMA actuators. Closed-loop control is realized by a proportional-integral (PI) controller with feed-forward compensation that processes the difference between desired and actual φ at a sampling rate of 200 Hz. K_s, K_p, K_i are feedforward gain, proportional gain and integral gain, respectively. **e**, The bending angle φ and duty ratio of SMA actuators as a function of time t when a desired step response is given. The actuation and deactivation response time are $t_a = 0.7$ s and $t_d = 4.6$ s, respectively.

motion. After 2.6 s, the bending angle reaches $\varphi = 154°$ (state II) and then the proportional-integral controller gradually reduces the duty ratio of SMA 2 (that is, decreasing the voltage) until the objective $\varphi = 230°$ is achieved (state III). Then the fan is activated to fully cool SMA 2 below A_f after 4.6 s (that is, deactivation time $t_d = 4.6$ s). At $t = 15$ s, SMA 1 is heated to contract. The backlash decreases to zero within 1.2 s (state V) and the detected φ begins to drop. Later, the duty ratio of SMA 1 is gradually reduced until φ reaches zero. Further cooling SMA 1 eliminates the contracting force of SMA 1 and recovers its initial state (state I). We also validate the closed-loop control by setting the desired objective as incremental step response, linear response and cosine response in Supplementary Fig. 14.

Individual after a stroke validation

Human hands can perform several single FMSs (Fig. 5a) and continuous switches between them for complex tasks (Fig. 5b). According to refs. 60–63, up to 90% of finger activities involve following six single FMSs: thumb opposition, tip pinch, tripod pinch, cylindrical pinch, lateral pinch and fist (Fig. 5a). We first calibrate the bending angles of involved fingers in these six single FMSs. Figure 5b shows a

https://doi.org/10.1038/s42256-023-00728-z

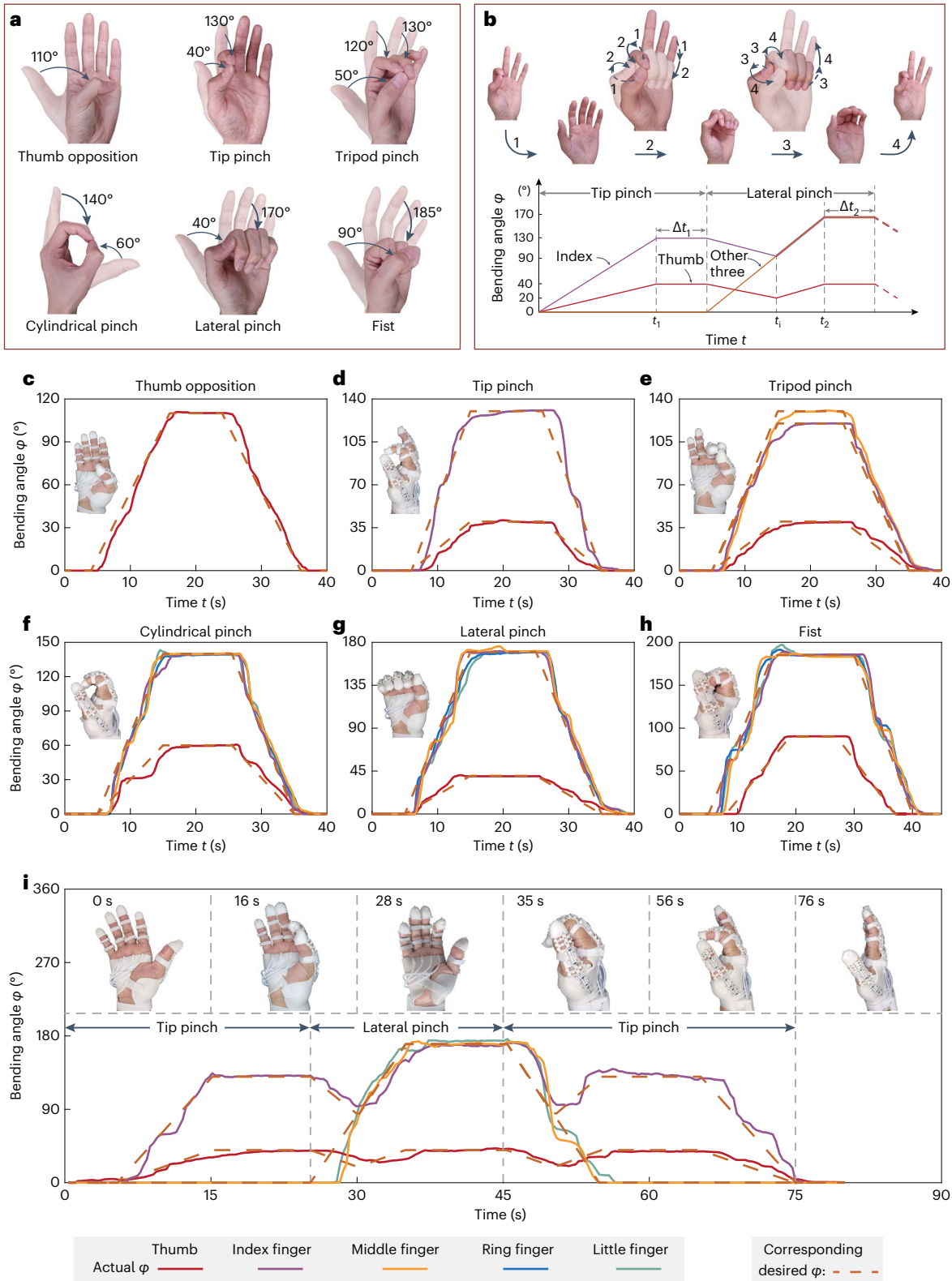

Fig. 5 | FMS rehabilitation on an individual after a stroke with an impaired hand. a, Illustration of six single-mode FMSs: thumb opposition, tip pinch, tripod pinch, cylindrical pinch, lateral pinch and fist. Bending angles of the involved fingers are provided near the gesture with arrows denoting the motion direction. **b**, Representative switch-mode FMS: tip pinch to lateral to tip pinch and the corresponding control scheme for five fingers. **c**–**h**, Comparison between desired and actual bending angles in six single-mode FMS rehabilitations: thumb opposition (**c**), tip pinch (**d**), tripod pinch (**e**), cylindrical pinch (**f**), lateral pinch (**g**) and fist (**h**). **i**, Representative switch-mode FMS rehabilitation from tip pinch to lateral pinch to tip pinch. The solid curves represent the actual bending angle of the involved fingers and the dashed brown curves show the corresponding desired bending angles.

representative switch-mode FMS: tip pinch to lateral pitch to tip pitch. The numbers 1 to 4 represent the motion sequence with arrows denoting the motion direction. A key aspect of the switching process is that the bent finger switches at an intermediate state rather than when the finger fully flattens. For example, in tip pinch to lateral pinch (Fig. 5b), the index and thumb fingers first bend to 130° and 40° at $t = t_1$ while the other three fingers remain flat. After a holding time Δt_1, the index and thumb finger gradually flatten to 90° and 20°, respectively. Meanwhile, the other three fingers bend to 90° at an intermediate time denoted as $t = t_i$. Thereafter, five fingers bend together and 40° is reached again by the thumb while 170° is achieved by the other fingers at $t = t_2$. Further switching activities can be performed after a holding time Δt_2 as illustrated by the dashed ending.

We first validate our soft glove on an individual with a normal hand. During the test, two myoelectric sensors are placed on the forearm to guarantee that the individual does not actively apply force to the finger, leaving the finger solely controlled by the soft glove. By selecting the single-mode module on the HMI panel, the individual can precisely finish the six single-mode FMSs (Supplementary Fig. 15 and Supplementary Video 6). Similarly, different switch-mode FMSs can also be accurately completed (Supplementary Fig. 16 and Supplementary Video 7). We then recruit an individual after a stroke (male, age 51) for validation. The individual had an ischaemic stroke (small ischaemic foci in bilateral frontal lobes) and now experiences impaired functions on the right hand. Specifically, his fingers are still a bit flaccid with some spasticity, that is, weak muscles are becoming stiff. His fingers can move with a small degree of freedom, but it is still hard for him to coordinate multiple fingers. This stage was characterized as Brunnstrom Stage II in the hospital. FMS rehabilitation at this stage plays an important role in reconstructing the correct and coordinated neural pathways[64]. To help him perform FMS rehabilitation, we first customize and fabricate a soft glove that fits his impaired hand. Rehabilitation outcomes are presented in Fig. 5c–i and Supplementary Fig. 17 in which the solid curves represent the actual bending angles of involved fingers and dashed brown curves are the corresponding desired bending angles. A comparison between single-mode and switch-mode FMS with and without the rehabilitation glove is provided in Supplementary Videos 8 and 9, respectively. Clearly, the actual bending angles agree well with the desired angles with small deviations. Such small deviations are due to the abnormal and uncontrollable muscle reactions from the individual after a stroke during the rehabilitation exercises. But deviations are usually eliminated within 2 s by the control system, that is, the disturbance from the individual can be automatically corrected by the closed-loop controllability. The transitions from one single mode to another are smooth and continuous. By adjusting the bending rate for different fingers, involved fingers can reach the desired bending angle simultaneously, suggesting the precise control and coordination of FMS rehabilitation.

Enabled by the light weight and high portability, our soft glove can provide highly repetitive and consistent FMS rehabilitation in various environments (Fig. 6a). For example, aside from the home, the individual can also do the rehabilitation while hanging out in the park. The soft glove not only provides rehabilitation to restore FMSs but also helps the individual with some activities of daily living (Supplementary Video 10). For example, Fig. 6b shows some representative daily activities that only require a single-mode FMS: dialling a phone (thumb opposition), combing (cylindrical pinch), brushing teeth (fist) and inserting a card (lateral pinch). Furthermore, the switch-mode FMS also assists the individual to finish some complex daily tasks. Figure 6c shows the image sequences in which the individual tears a snack wrapper and then holds it to eat. The required FMSs are tip pinch to cylindrical pinch. Figure 6d shows that the individual fills a cup with water and takes pills. The required FMSs are from the fist to the tip pinch. Figure 6e presents that the individual first picks the pen, presses the pen button and writes. The involved FMSs are tip pinch to lateral pinch to tripod pinch.

Discussion

Recovering FMSs in hand rehabilitation has been a long-standing challenge due to the lack of sensing of finger movement and a closed-loop control algorithm in existing rehabilitation gloves. Here we have engineered a soft-packaged rehabilitation glove with tight integration of sensing, actuation, HMI, power, electronics and a closed-loop algorithm. This rehabilitation glove allows patients after a stroke to recover the FMSs of the fingers in a portable manner. Note that our soft glove is still in development, and the following aspects should be considered before it is used in applications. First, our soft glove is more suitable for patients with muscle weakness or low rigidity (that is, patients during Brunnstrom Stages I and II). For these patients, the soft glove can assist them to finish FMS rehabilitation with high precision, facilitating the reconstruction of the correct neural pathway. On the contrary, for patients with high muscle rigidity (hypertonia), the driving force by heated SMA may not be sufficient to deform their 'frozen' fingers. In this regard, we suggest a complete evaluation of the muscle strength and performance of patients before using the soft glove. Second, there are no comprehensive data to validate the long-lasting rehabilitation outcome of our soft glove. During the COVID-19 pandemic, most hospitals in China had limited capacity and we had limited access to patients after a stroke who may test our soft glove. Statistical analysis on more participants with control groups can be carried out in the future. Third, the active involvement of patients in executing rehabilitation exercises has a critical role in empowering cortical reorganization after a stroke. We are committed to developing a next-generation soft glove that has more active involvement of patients.

Methods

Fabrication of soft glove

Three-dimensional (3D) computer-aided design models of fingerstalls and soft palm are first built according to the hand size of the wearer of interest. Then, they are fabricated by a moulding process (Wenext Company). The soft material used is a polyurethane (8400)-based rubber that holds high elasticity and softness within temperatures ranging from −10 °C to 80 °C. The Shore hardness of the fingerstalls and the palm is 40 HA and 60 HA, respectively. The SMA actuators are fixed to the arm fixation by riveting. The arm fixation, the wrist fixation, the bottom plate and the upper cover plate are fabricated by 3D printing. The fan is attached to the upper cover plate and its maximum power is 17.4 W. Five motors are assembled on the upper cover to selectively control the airway switches. The cable sheaths are Teflon tubes with an outer diameter of 2.8 mm and an inner diameter of 1.8 mm. Ultrahigh-molecular-weight polyethylene fibre composite line (KaDiLai Company) is used for connecting wire, force wire and bending/flattening cables. The diameter of the composite line is 0.14 mm and the ultimate tensile strength is 76 N.

Mechanical characterization of SMA actuators

SMA actuators are TiNi-alloy springs (flexinol wire, Dynalloy). The diameter of the thin wire is 0.51 mm and the density is 6.45 g cm^{-3}. The outer diameter of the spring is 3.45 mm. The austenite phase finish temperature is 90 °C. Each SMA actuator has 50 coils and is pre-stretched to 100 mm as the initial length. Four steps are used to characterize its mechanical response in the closed temperature chamber of an electromechanical universal testing machine (Wance Company; maximum load 50 N). Step one: the SMA spring was stretched from 100 mm to 180 mm with a loading rate of 100 mm min^{-1} at a room temperature of 25 °C. Step two: the length of the SMA spring was fixed at 180 mm, and the temperature was increased from 25 °C to 90 °C. The total heating time is 1 h, during which the force is recorded at an interval of 2.5 °C. Step three: fixing the chamber temperature at 90 °C, the length of the SMA spring was gradually reduced to 100 mm with a loading rate of 100 mm min^{-1}. Step four: fixing the length of 100 mm, the temperature of the chamber was gradually cooled from 90 °C to 25 °C. The total

https://doi.org/10.1038/s42256-023-00728-z

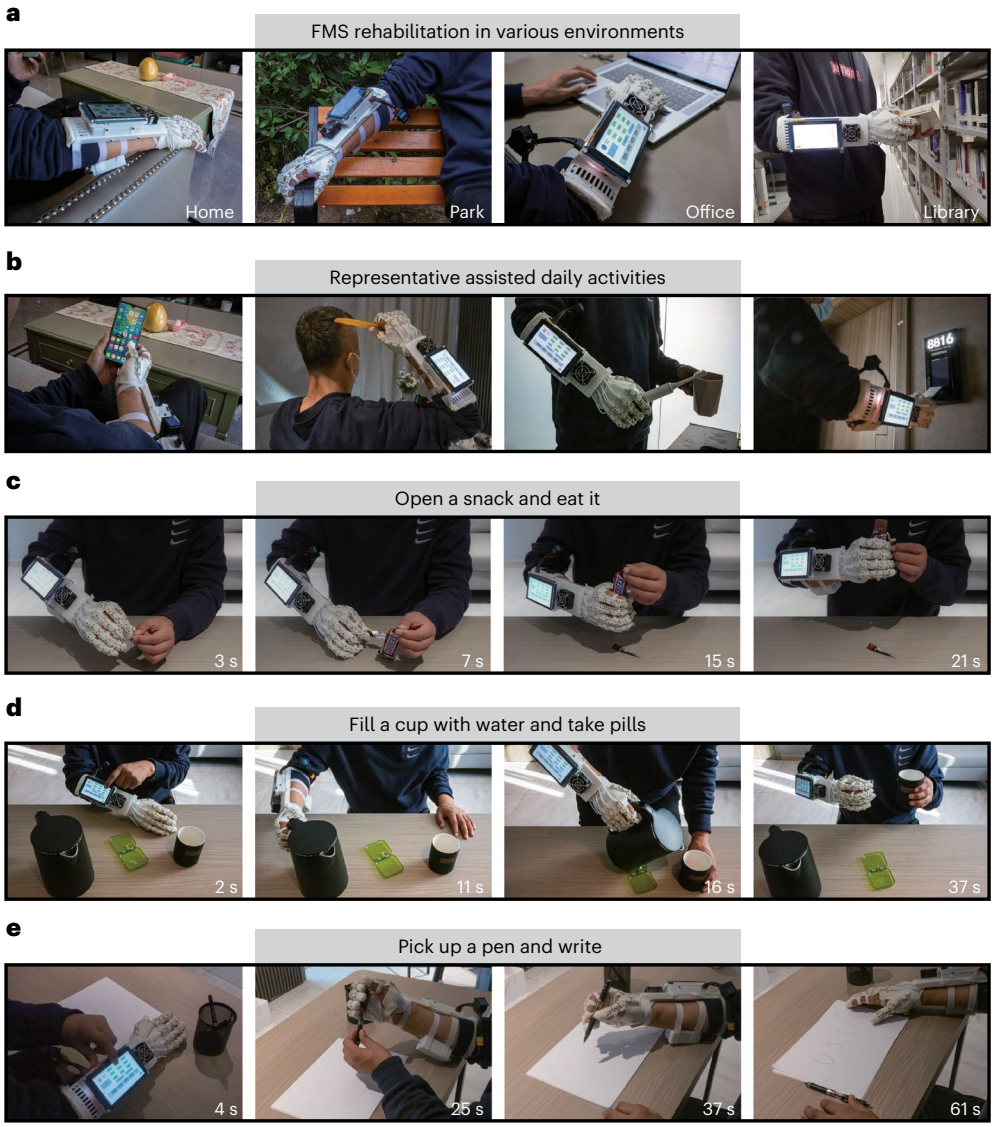

Fig. 6 | FMS rehabilitation and daily assistance for an individual after a stroke. a, Our soft glove can provide repetitive and consistent FMS rehabilitation in various environments such as at home, in a park, in an office and in a library. **b**, Representative daily activities assisted by our soft glove: dialling a phone (thumb opposition), combing (cylindrical pinch), brushing teeth (fist) and inserting a card (lateral pinch). **c**, Image sequences of opening a snack and holding it to eat. Required FMSs are tip pinch to cylindrical pinch. **d**, Image sequences of filling a cup with water and taking pills. Required FMSs are fist to tip pinch. **e**, Image sequences of picking up a pen, pressing the button and writing the USTC logo. Required FMSs are tip pinch to lateral pinch to tripod pinch.

cooling process took 1 h, during which the force is measured at intervals of 2.5 °C. Repeatability tests are performed by heating and cooling the SMA with different contraction ratios (SMA length varies between 10 cm and 18 cm) with a load of 7 N (equivalent stress 34 MPa). The length of the SMA is recorded by a displacement sensor in 10,000 cycles. Measurements of energy density and energy efficiency are performed by recording the input electric energy and the work done to lift a 7 N load.

Image-based calibration system

Four sets of LED lights were placed on the metacarpal area and the three phalangeal areas of the finger. The joint angles of MCP, PIP and DIP can be determined by the angle between two adjacent sets of LED lights. A camera (Mars2000-50gc, Hangzhou Weitu Vision Technology) was used to capture the bent finger with a frame rate of 20 Hz. The image was then analysed by using the MATLAB image processing toolbox. The finger phantom is fabricated by hinging 3D-printed phalanges (photopolymer resin white (FLGPWH04), Formlabs) and a thin layer of cover (EcoFlex, Smooth-On).

Bending sensors

The 30 Hall sensors (model A1302) used in 15 bending sensors are made by Allegro MicroSystems. The sensitivity of the Hall sensors is 1.3 mV G^{-1}. The N35 magnet has a dimension of 3.5 mm × 3.5 mm × 1.3 mm.

Sampling and control

The heart of the sampling and control is four 16-bit analogue-to-digital converters (model AD7606 from Analog Devices) with 8 channels and conversion rates up to 200 kSPS and a 32-bit microcontroller unit (MCU) model STM32 (STMicroelectronics). The output voltage is sampled at a rate of 200 Hz and then transmitted from the analogue-to-digital converter to the MCU through the serial peripheral interface (SPI) communication protocol and filtered in the MCU. The actual bending of the finger is then calculated according to the calibration results. A proportional-integral controller with feed-forward compensation then processes the difference between the actual and desired bending angles and transmits the control parameters to the driver circuit. Note that overheat protection is designed during data

transmission. If the control signal is transmitted continuously but the actual bending angle remains unchanged within 5 s, the system is automatically powered off.

Human–machine interface

A 4.3-inch touchable screen (Taojingchi Company) is used for display and interaction. Four functions are programmed into the HMI—(1) basic module of controlling each finger; (2) single-mode FMSs; (3) switch-mode of FMS; (4) daily assistance—and displayed in three layers. The bent states of all fingers can be set by typing on the first layer. Then, we can touch the button 'FMS list' to enter the second layer to select a single-mode FMS rehabilitation. Further, the third layer is accessed through the touchable button 'Switch modes'. On the third page, we can select 'Single mode' to enter a box named 'Switch sequence', then the button 'Rehabilitation' is pressed, and we can achieve the switch modes of FMS rehabilitation. When the button 'Daily assistance' is pressed, the soft glove can assist us with completing activities of daily living. Three preset buttons assist the individual to eat cookies, take pills and write (Supplementary Video 10).

Power management

A lithium battery with a capacity of 2,000 mAh and a size of 24 mm × 31 mm × 73 mm is adopted as the power. The voltage is 12 V and the discharge rate is 20 C. Due to the different voltages required by each module, the step-down chip (model TPS54302DDCR, Texas Instruments) is used to obtain a voltage of 5 V to power the Hall sensors and PCA9685, and then a voltage of 3.3 V is converted by low dropout voltage regulator model AMS1117 (Slkor Company) to power the MCU.

Driver circuit and actuator

The control parameters from the MCU are received by a 12-bit PWM wave generator (PCA9685, NXP Semiconductors) through an inter-integrated circuit (I2C) bus. Then ten-channel PWM waves are amplified in the drive circuit to drive the SMA actuators. The high-current circuit and the control circuit are isolated by an optical coupler to avoid interference between them.

Finite element analysis

FEA is performed by using the commercial package Abaqus Standard 2019. The serpentine structures are modelled as a two-dimensional shell with plane strain conditions. The finger joints are assumed to be rigid arcs with different radii and angles (labelled in Fig. 2d). The left boundary of the serpentine structure is clamped while the right boundary is stretched by a force until the rigid arc is fully covered by the serpentine structure. The interaction between the serpentine structure and the rigid arc is frictionless without penetration.

Human research participants and ethics

The recruited individual after a stroke is a 51-year-old Chinese male and consented to all the experiments and identifiable images in this work with reasonable compensations. Rehabilitation exercises on the individual were conducted by protocols approved by the Ethical Committee of The First Affiliated Hospital of University of Science and Technology of China (number 2022KY276).

Reporting summary

Further information on research design is available in the Nature Portfolio Reporting Summary linked to this article.

Data availability

The authors declare that the main data supporting the findings of this study are available within the article and its Supplementary Information files. Other data, if needed, can be available upon request.

Code availability

All the relevant codes are available at https://github.com/weibayang/rehabilitation_glove (ref. 65).

References

1. Cao, D. et al. Efficacy and safety of manual acupuncture for the treatment of upper limb motor dysfunction after stroke: protocol for a systematic review and meta-analysis. *PLoS ONE* **16**, e0258921 (2021).
2. Sobinov, A. R. & Bensmaia, S. J. The neural mechanisms of manual dexterity. *Nat. Rev. Neurosci.* **22**, 741–757 (2021).
3. Yavuzer, G. et al. Mirror therapy improves hand function in subacute stroke: a randomized controlled trial. *Arch. Phys. Med. Rehabil.* **89**, 393–398 (2008).
4. Pereira, M. F., Prahm, C., Kolbenschlag, J., Oliveira, E. & Rodrigues, N. F. Application of AR and VR in hand rehabilitation: a systematic review. *J. Biomed. Inform.* **111**, 103584 (2020).
5. Draganski, B. et al. Neuroplasticity: changes in grey matter induced by training. *Nature* **427**, 311–312 (2004).
6. Harvey, R. L. Improving poststroke recovery: neuroplasticity and task-oriented training. *Curr. Treat. Options Cardiovasc. Med.* **11**, 251–259 (2009).
7. Keller, J. L. et al. Thirty years of hand therapy: the 2014 practice analysis. *J. Hand Ther.* **29**, 222–234 (2016).
8. Zollo, L., Accoto, D., Sterzi, S. & Guglielmelli, E. *Springer Handbook of Medical Technology* (eds Kramme, R., et al.) Ch. 42 (Springer, 2011).
9. van Stormbroek, K. & Buchanan, H. Novice therapists in a developing context: extending the reach of hand rehabilitation. *Hand Ther.* **22**, 141–152 (2017).
10. Leonardis, D. et al. An EMG-controlled robotic hand exoskeleton for bilateral rehabilitation. *IEEE Trans. Haptics* **8**, 140–151 (2015).
11. Yang, G. Z., Riener, R. & Dario, P. To integrate and to empower: robots for rehabilitation and assistance. *Sci. Robot.* **2**, eaan5593 (2017).
12. Dupont, P. E. et al. A decade retrospective of medical robotics research from 2010 to 2020. *Sci. Robot.* **6**, eabi8017 (2021).
13. Borboni, A., Mor, M. & Faglia, R. Gloreha—hand robotic rehabilitation: design, mechanical model, and experiments. *J. Dyn. Syst. Meas. Control.* **138**, 111003 (2016).
14. Baniqued, P. D. E. et al. Brain–computer interface robotics for hand rehabilitation after stroke: a systematic review. *J. Neuroeng. Rehabil.* **18**, 15 (2021).
15. Lum, P. S., Godfrey, S. B., Brokaw, E. B., Holley, R. J. & Nichols, D. Robotic approaches for rehabilitation of hand function after stroke. *Am. J. Phys. Med.* **91**, S242–S254 (2012).
16. Torrisi, M. et al. Beyond motor recovery after stroke: the role of hand robotic rehabilitation plus virtual reality in improving cognitive function. *J. Clin. Neurosci.* **92**, 11–16 (2021).
17. Noronha, B. & Accoto, D. Exoskeletal devices for hand assistance and rehabilitation: a comprehensive analysis of state-of-the-art technologies. *IEEE Trans. Med. Robot. Bionics* **3**, 525–538 (2021).
18. Sandoval-Gonzalez, O. et al. Design and development of a Hand exoskeleton robot for active and passive rehabilitation. *Int. J. Adv. Robot. Syst.* **13**, 1–12 (2016).
19. Lambercy, O. et al. A haptic knob for rehabilitation of hand function. *IEEE Trans. Neural Syst. Rehabil. Eng.* **15**, 356–366 (2007).
20. Maciejasz, P., Eschweiler, J., Gerlach-Hahn, K., Jansen-Troy, A. & Leonhardt, S. A survey on robotic devices for upper limb rehabilitation. *J. Neuroeng. Rehabil.* **11**, 3 (2014).
21. Laschi, C., Mazzolai, B. & Cianchetti, M. Soft robotics: technologies and systems pushing the boundaries of robot abilities. *Sci. Robot.* **1**, eaah3690 (2016).
22. Gorissen, B. et al. Elastic inflatable actuators for soft robotic applications. *Adv. Mater.* **29**, 1604977 (2017).

23. Yang, G. Z. et al. The grand challenges of science robotics. *Sci. Robot.* **3**, eaar7650 (2018).
24. Shahid, T., Gouwanda, D., Nurzaman, S. G. & Gopalai, A. A. Moving toward soft robotics: a decade review of the design of hand exoskeletons. *Biomimetics* **3**, 17 (2018).
25. Zhang, Y. & Lu, M. A review of recent advancements in soft and flexible robots for medical applications. *Int. J. Med. Robotics. Comput. Assist. Surg.* **16**, e2096 (2020).
26. Gul, J. Z. et al. 3D printing for soft robotics—a review. *Sci. Technol. Adv. Mater.* **19**, 243–262 (2018).
27. Sanchez, V., Walsh, C. J. & Wood, R. J. Textile technology for soft robotic and autonomous garments. *Adv. Funct. Mater.* **31**, 2008278 (2021).
28. Polygerinos, P., Wang, Z., Galloway, K. C., Wood, R. J. & Walsh, C. J. Soft robotic glove for combined assistance and at-home rehabilitation. *Rob. Auton. Syst.* **73**, 135–143 (2015).
29. Yap, H. K. et al. A fully fabric-based bidirectional soft robotic glove for assistance and rehabilitation of hand impaired patients. *IEEE Robot. Autom. Lett.* **2**, 1383–1390 (2017).
30. Wang, J., Fei, Y. & Pang, W. Design, modeling, and testing of a soft pneumatic glove with segmented pneuNets bending actuators. *IEEE ASME Trans. Mechatron.* **24**, 990–1001 (2019).
31. Feng, M., Yang, D. & Gu, G. High-force fabric-based pneumatic actuators with asymmetric chambers and interference-reinforced structure for soft wearable assistive gloves. *IEEE Robot. Autom. Lett.* **6**, 3105–3111 (2021).
32. Tang, Z. Q., Heung, H. L., Tong, K. Y. & Li, Z. Model-based online learning and adaptive control for a 'human-wearable soft robot' integrated system. *Int. J. Rob. Res.* **40**, 256–276 (2021).
33. Li, H., Cheng, L., Li, Z. & Xue, W. Active disturbance rejection control for a fluid-driven hand rehabilitation device. *IEEE ASME Trans. Mechatron.* **26**, 841–853 (2021).
34. Ge, L. et al. Design, modeling, and evaluation of fabric-based pneumatic actuators for soft wearable assistive gloves. *Soft Robot.* **7**, 583–596 (2020).
35. Popov, D., Gaponov, I. & Ryu, J. H. Portable exoskeleton glove with soft structure for hand assistance in activities of daily living. *IEEE ASME Trans. Mechatron.* **22**, 865–875 (2017).
36. Chen, X. et al. A wearable hand rehabilitation system with soft gloves. *IEEE Trans. Industr. Inform.* **17**, 943–952 (2021).
37. Xiloyannis, M., Cappello, L., Khanh, D. B., Yen, S. C. & Masia, L. Modelling and design of a synergy-based actuator for a tendon-driven soft robotic glove. In *6th IEEE International Conference on Biomedical Robotics and Biomechatronics* 1213–1219 (IEEE, 2016).
38. Nycz, C. J. et al. Design and characterization of a lightweight and fully portable remote actuation system for use with a hand exoskeleton. *IEEE Robot. Autom. Lett.* **1**, 976–983 (2016).
39. Kang, B. B., Choi, H., Lee, H. & Cho, K. J. Exo-Glove Poly II: a polymer-based soft wearable robot for the hand with a tendon-driven actuation system. *Soft Robot.* **6**, 214–227 (2019).
40. Dragusanu, M., Iqbal, M. Z., Baldi, T. L., Prattichizzo, D. & Malvezzi, M. Design, development, and control of a hand/wrist exoskeleton for rehabilitation and training. *IEEE Trans. Robot.* **38**, 1472–1488 (2022).
41. Tran, P. et al. FLEXotendon Glove-III: voice-controlled soft robotic hand exoskeleton with novel fabrication method and admittance grasping control. *IEEE ASME Trans. Mechatron.* **27**, 3920–3931 (2022).
42. Chen, W. et al. Soft exoskeleton with fully actuated thumb movements for grasping assistance. *IEEE Trans. Robot.* **38**, 2194–2207 (2022).
43. Huang, X. et al. Chasing biomimetic locomotion speeds: creating untethered soft robots with shape memory alloy actuators. *Sci. Robot.* **3**, eaau7557 (2018).
44. Yang, X., Chang, L. & Perez-Arancibia, N. O. An 88-milligram insect-scale autonomous crawling robot driven by a catalytic artificial muscle. *Sci. Robot.* **5**, eaba0015 (2020).
45. Rodrigue, H., Wang, W., Han, M. W., Kim, T. J. Y. & Ahn, S. H. An overview of shape memory alloy-coupled actuators and robots. *Soft Robot.* **4**, 3–15 (2017).
46. Jeong, J. et al. Wrist assisting soft wearable robot with stretchable coolant vessel integrated SMA muscle. *IEEE ASME Trans. Mechatron.* **27**, 1046–1058 (2022).
47. Wang, W., Yu, C. Y., Abrego Serrano, P. A. & Ahn, S. H. Shape memory alloy-based soft finger with changeable bending length using targeted variable stiffness. *Soft Robot.* **7**, 283–291 (2020).
48. Nguyen, X.-T., Calderon, A. A., Rigo, A., Ge, J. Z. & Perez-Arancibia, N. O. SMALLBug: a 30-mg crawling robot driven by a high-frequency flexible SMA microactuator. *IEEE Robot. Autom. Lett.* **5**, 6796–6803 (2020).
49. Park, S. J., Kim, U. & Park, C. H. A novel fabric muscle based on shape memory alloy springs. *Soft Robot.* **7**, 321–331 (2020).
50. Yang, H., Xu, M., Li, W. & Zhang, S. Design and implementation of a soft robotic arm driven by SMA coils. *IEEE Trans. Ind. Electron.* **66**, 6108–6116 (2019).
51. Jin, H. et al. Modeling and motion control of a soft SMA planar actuator. *IEEE ASME Trans. Mechatron.* **27**, 916–927 (2022).
52. Hadi, A., Alipour, K., Kazeminasab, S. & Elahinia, M. ASR glove: a wearable glove for hand assistance and rehabilitation using shape memory alloys. *J. Intell. Mater. Syst. Struct.* **29**, 1575–1585 (2018).
53. Copaci, D., Arias, J., Gomez-Tome, M., Moreno, L. & Blanco, D. sEMG-based gesture classifier for a rehabilitation glove. *Front. Neurorobot.* **16**, 750482 (2022).
54. Tran, P., Jeong, S., Herrin, K. R. & Desai, J. P. Hand exoskeleton systems, clinical rehabilitation practices, and future prospects. *IEEE Trans. Med. Robot. Bionics* **3**, 606–622 (2021).
55. Zhang, D. R. et al. Real-time performance of hand motion recognition using kinematic signals for impaired hand function training. In *6th International IEEE EMBS Conference on Neural Engineering* 339–342 (IEEE, 2013).
56. Liu, X. et al. Design of virtual guiding tasks with haptic feedback for assessing the wrist motor function of patients with upper motor neuron lesions. *IEEE Trans. Neural Syst. Rehabil. Eng.* **27**, 984–994 (2019).
57. Dana, A., Vollach, S. & Shilo, D. Use the force: review of high-rate actuation of shape memory alloys. *Actuators* **10**, 7 (2021).
58. Lagoudas, D. C. *Shape Memory Alloys: Modeling and Engineering Applications* (ed Lagoudas, D.) Ch. 1 (Springer, 2008).
59. Neumann, D. *Kinesiology of the Musculoskeletal System: Foundation for Rehabilitation* (ed Neumann, D.) Ch. 8 (Elsevier Mosby, 2016).
60. Kyberd, P. J. & Pons, J. L. A comparison of the Oxford and Manus intelligent hand prostheses. In *20th IEEE International Conference on Robotics and Automation* 3231–3236 (IEEE, 2003).
61. Iberall, T. Human prehension and dexterous robot hands. *Int. J. Rob. Res.* **16**, 285–299 (1997).
62. Cutkosky, M. R. & Wright, P. K. Modelling manufacturing grips and correlations with the design of robotic hands. In *1986 IEEE International Conference on Robotics and Automation* 1533–1539 (IEEE, 1986).
63. Ciancio, A. L., Zollo, L., Baldassarre, G., Caligiore, D. & Guglielmelli, E. The role of thumb opposition in cyclic manipulation: a study with two different robotic hands. In *4th IEEE RAS-EMBS International Conference on Biomedical Robotics and Biomechatronics* 1092–1097 (IEEE, 2012).
64. Li, S. Spasticity, motor recovery, and neural plasticity after stroke. *Front. Neurol.* **8**, 120 (2017).

65. Sui, M et al. A soft-packaged and portable rehabilitation glove capable of closed-loop fine motor skills. *Zenodo* https://doi.org/10.5281/zenodo.8172352 (2023).

Acknowledgements

This work is supported by National Natural Science Foundation of China (numbers 51975550, U21A20119, 12272369 and 51705495), National Key Research and Development Program of China (number 2022YFC2408100), Provincial Key Research and Development Program of Anhui Province (number 202104h04020004), Natural Science Foundation of Anhui Province of China under Grant 2008085UD02, and Fundamental Research Funds for the Central Universities (WK5290000002).

Author contributions

Conceptualization: M.S., H.J., L.W. and S.Z. Methodology: M.S., Y.O., H.J., Z.C. and C.W. Investigation: M.S., Y.O., H.J., Z.C., C.W. and J.L. Visualization: M.S., Y.O., H.J., J.L., L.W. and S.Z. Funding acquisition: H.J., L.W. and S.Z. Project administration: H.J., L.W. and S.Z. Supervision: H.J., L.W. and S.Z. Writing—original draft: M.S., H.J. and L.W. Writing—review and editing: M.S., H.J., M.X., W.L., L.W. and S.Z.

Competing interests

M.S., Y.O., H.J. and S.Z. are inventors of an invention disclosure of the patent filed by University of Science and Technology of China (ZL202011284541.3, granted on 13 May 2022) related to this work. The other authors declare no competing interests.

Additional information

Supplementary information The online version contains supplementary material available at https://doi.org/10.1038/s42256-023-00728-z.

Correspondence and requests for materials should be addressed to Hu Jin, Liu Wang or Shiwu Zhang.

Peer review information *Nature Machine Intelligence* thanks Xiaonan Huang for their contribution to the peer review of this work. Primary Handling Editor: Trenton Jerde, in collaboration with the *Nature Machine Intelligence* editorial team.

nature portfolio

Corresponding author(s): Hu Jin, Liu Wang, Shiwu Zhang
NATMACHINTELL-A22116916C

Last updated by author(s): Aug 22, 2023

Reporting Summary

Nature Portfolio wishes to improve the reproducibility of the work that we publish. This form provides structure for consistency and transparency in reporting. For further information on Nature Portfolio policies, see our Editorial Policies and the Editorial Policy Checklist.

Statistics

For all statistical analyses, confirm that the following items are present in the figure legend, table legend, main text, or Methods section.

n/a	Confirmed
☒	☐ The exact sample size (*n*) for each experimental group/condition, given as a discrete number and unit of measurement
☒	☐ A statement on whether measurements were taken from distinct samples or whether the same sample was measured repeatedly
☒	☐ The statistical test(s) used AND whether they are one- or two-sided *Only common tests should be described solely by name; describe more complex techniques in the Methods section.*
☒	☐ A description of all covariates tested
☒	☐ A description of any assumptions or corrections, such as tests of normality and adjustment for multiple comparisons
☒	☐ A full description of the statistical parameters including central tendency (e.g. means) or other basic estimates (e.g. regression coefficient) AND variation (e.g. standard deviation) or associated estimates of uncertainty (e.g. confidence intervals)
☒	☐ For null hypothesis testing, the test statistic (e.g. *F*, *t*, *r*) with confidence intervals, effect sizes, degrees of freedom and *P* value noted *Give P values as exact values whenever suitable.*
☒	☐ For Bayesian analysis, information on the choice of priors and Markov chain Monte Carlo settings
☒	☐ For hierarchical and complex designs, identification of the appropriate level for tests and full reporting of outcomes
☒	☐ Estimates of effect sizes (e.g. Cohen's *d*, Pearson's *r*), indicating how they were calculated

Our web collection on statistics for biologists contains articles on many of the points above.

Software and code

Policy information about availability of computer code

Data collection	Halcon 12.0 is used for collecting the motion information of fingers in image-base calibration system. Keil 5.0 is used for collecting the voltage of the bending sensors.
Data analysis	MATLAB R2020b is used for data analysis.

For manuscripts utilizing custom algorithms or software that are central to the research but not yet described in published literature, software must be made available to editors and reviewers. We strongly encourage code deposition in a community repository (e.g. GitHub). See the Nature Portfolio guidelines for submitting code & software for further information.

Data

Policy information about availability of data

All manuscripts must include a data availability statement. This statement should provide the following information, where applicable:

- Accession codes, unique identifiers, or web links for publicly available datasets
- A description of any restrictions on data availability
- For clinical datasets or third party data, please ensure that the statement adheres to our policy

The main data supporting the findings of this study are available within the article and its Supplementary Information files.

Human research participants

Policy information about studies involving human research participants and Sex and Gender in Research.

Reporting on sex and gender	Male
Population characteristics	The participant(age 51) had an is chemic stroke (small ischemic foci in bilateral frontal lobes) and now experiences impaired functions on the right hand. Specifically, his fingers are still a bit flaccid with some spasticity, i.e., weak muscles are becoming stiff. And his fingers can move with a small degree of freedom, but it is still hard for him to coordinate multiple fingers. This stage was characterized as Brunnstrom Stage II in the hospital.
Recruitment	Participants was recruited openly in this research and there was no self-selection bias and other biases.
Ethics oversight	Approved by the Ethical Committee of The First Affiliated Hospital of University of Science and Technology of China (number: 2022KY276)

Note that full information on the approval of the study protocol must also be provided in the manuscript.

Field-specific reporting

Please select the one below that is the best fit for your research. If you are not sure, read the appropriate sections before making your selection.

☒ Life sciences ☐ Behavioural & social sciences ☐ Ecological, evolutionary & environmental sciences

For a reference copy of the document with all sections, see nature.com/documents/nr-reporting-summary-flat.pdf

Life sciences study design

All studies must disclose on these points even when the disclosure is negative.

Sample size	During the Covid-19 pandemic, most hospitals in China has limited capacity and we had limited access to poststroke patients who may test our soft glove. Statistical analysis on more participants with control groups can be carried out in the future.
Data exclusions	Gross errors were excluded.
Replication	The reliability of the bending sensors was verified by 50 repeated experiments.
Randomization	Participants were recruited randomly, without self-selection by the authors.
Blinding	The research had only one group because of the Covid-19 pandemic.

Reporting for specific materials, systems and methods

We require information from authors about some types of materials, experimental systems and methods used in many studies. Here, indicate whether each material, system or method listed is relevant to your study. If you are not sure if a list item applies to your research, read the appropriate section before selecting a response.

Materials & experimental systems

n/a	Involved in the study
☒	☐ Antibodies
☒	☐ Eukaryotic cell lines
☒	☐ Palaeontology and archaeology
☒	☐ Animals and other organisms
☒	☐ Clinical data
☒	☐ Dual use research of concern

Methods

n/a	Involved in the study
☒	☐ ChIP-seq
☒	☐ Flow cytometry
☒	☐ MRI-based neuroimaging